Astron. Astrophys. 241, 375–388 (1991)

ASTRONOMY AND ASTROPHYSICS

A detailed study of the ionized hydrogen distribution and of the velocity field of the barred galaxy NGC 7741

M.F. Duval [1], G. Monnet [2], J. Boulesteix [1], Y. Georgelin [1], E. Le Coarer [1], and M. Marcelin [1]

[1] Observatoire de Marseille, 2 Place Le Verrier, F-13248 Marseille Cedex 04, France
[2] Canada-France-Hawaii Telescope, P.O. Box 1597, Kamuela, HI 96743, USA

Received March 24, 1989; accepted July 27, 1990

Abstract. A photometric catalogue of 306 H II regions of NGC 7741 is presented with an analysis of the distribution of the fluxes. 2500 radial velocities of the ionized gas have then been measured with a scanning Pérot-Fabry interferometer and a two-dimensional counting system. A dynamical model is derived, which reasonably fits the velocity field, for a bar to disk mass-ratio inside the radius of the bar of roughly 30%.

Key words: barred galaxies – kinematics and dynamics of galaxies

1. Introduction

In a previous paper (Duval & Monnet 1985, hereafter DM) we published a preliminary velocity field of the H II regions of NGC 7741, obtained from six long-slit spectra. A B isophotal map was used to separate three components, the extended disk, the central disk and the bar. The velocity field did exhibit (as well as for the two other barred spirals studied in that paper) a clear S-shaped distortion related to the bar as predicted by Kalnajs (1978). A crude analysis of the velocity field was used to derive the blue (M/L) ratio of the stellar bar which was found close to that of the surrounding disk.

We have since obtained a new velocity field more accurate and with a much better spatial coverage, through the use of a scanning Fabry-Pérot interferometer working at Hα. It is presented in Part 3. A less simple dynamical analysis than in DM was then obviously needed. We made 2D hydrodynamical models of the gas flow in the potential of the galaxy, which are compared to the observed velocity field. Furthermore, a photometric study of H II regions has been made (Part 2) and they are catalogued. If a detailed catalogue of H II regions have now been published for quite a number of SA or SAB galaxies, e.g. M31, M33, NGC 628, NGC 2997, NGC 1566, M83, NGC 6946, NGC 300 (see Deharveng et al. 1988 for references) and M81 (Petit et al. 1988), but very few concern barred spirals. The only example is NGC 1313 (Marcelin & Gondoin 1983). These H II regions photometric data are then used to constrain the dynamical model given in Part 3.

For a better view of the photometric and kinematic aspects, we have summarized in Table 1 the global properties of the galaxy (more detailed parameters can be found in DM). The center of NGC 7741 is relatively difficult to find, as no central bulge can be seen. Following G. de Vaucouleurs' prescriptions, we choose in the midst of the bar the local minimum in blue and Hα light. This point, offset by 7″ from the center of the bar, is also the center of the asymmetric stellar continuum distribution.

Table 1. Physical data of NGC 7741

	Ref. 1 [a]	Ref. 2 [b]
Equatorial coordinates of the center (1950)	$\alpha = 23^h41^m22^s.6$ $\delta = 25°47'54''.2$	
Corrected apparent magnitude [c]	$B_T^0 = 11.41$	11.69
Corrected absolute magnitude	$M_T^0(B) = -18.70$	−18.76
Distance moduli	$\mu_T^0 = 30.11$	30.45
Corrected total blue luminosity	$L_T^0/L_\odot = 4.4\ 10^9$	$5.0\ 10^9$
Inclination	$i = 45° \pm 2°$	51°
Bar position angle	$\theta = 98° \pm 2°$	
Axis ratio of the bar	$b/a = 0.30 \pm 0.02$	
Major axis position angle of the extended disk	$160 \pm 5°$ E	

[a] Duval & Monnet (1985)
[b] Tully (1988, Nearby Galaxies Catalogue, GCT)
[c] 0.18 of the difference comes from the galactic absorption coefficient (0.31 in RC2 and 0.13 in GCT)

2. Photometric study of the H II regions

2.1. Observations and reductions

The Hα images have been obtained by J. Boulesteix, G. Courtès, and H. Petit at the prime focus of the 6-m telescope of the Soviet Special Astrophysical Observatory in Zelenchuk equipped with the large focal reducer of Courtès and a RCA image tube. With an aperture ratio of f:1.6, the scale on the plates is 24″.2 mm^{-1}. The interference filter centered at 658.55 nm had a very small FWHM of 0.6 nm. The exposure times were 5 and 15 min (Fig. 1)

Send offprint requests to: M. F. Duval

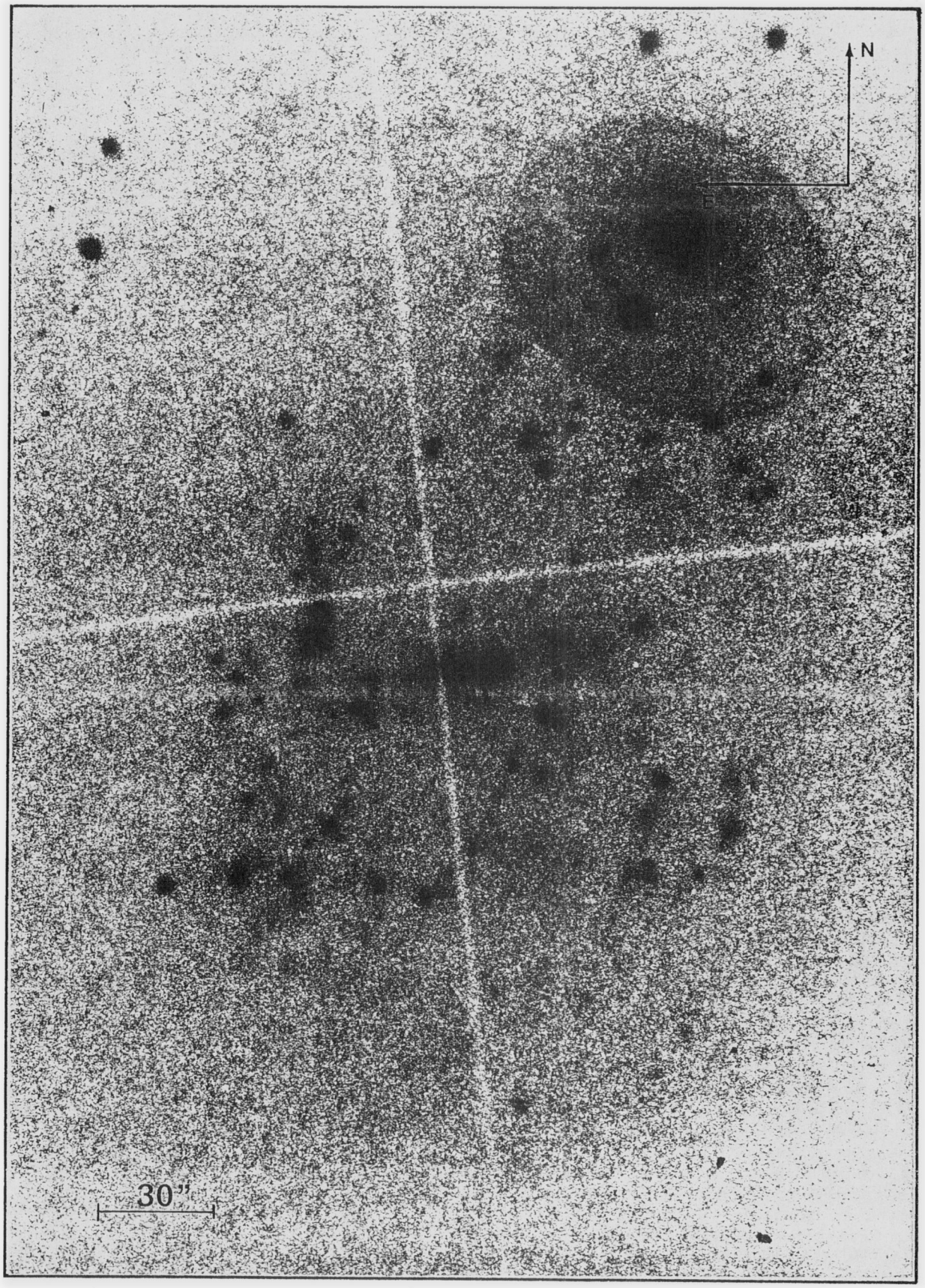

Fig. 1. Hα exposure of NGC 7741 on IIaO plate (15 min), taken with the 6-m telescope of the Soviet Special Astrophysical Observatory in Zelenchuk

on IIaO plates. Four other plates in the B and V spectral ranges taken at the Newton focus of the Haute-Provence 1.2 meter telescope and already used for surface photometry of the galaxy (DM) were used to avoid continuum sources in the catalogue.

These plates have been scanned with the PDS photodensitometer of the Laboratoire d'Astronomie Spatiale with a square slit of 60 μm side (1″.5 on the sky) and a 40 μm sampling step. The measurements of the H II regions presented the usual difficulties relative to the background determination. In our case, it was the contribution of the sky and image tube noises and the continuum light of star clusters belonging to the H II regions or very close to them.

We choose to measure the total flux above a well defined background (sky + image tube noise) estimated on the whole plate from outer regions with a smoothing algorithm. This does not allow the subtraction of the stellar continuum, which however is estimated to be not greater than 5 to 10% of the total flux of any H II region, depending of the localization.

2.2. *Diameters*

Equivalent diameters have been obtained by the formula:

$$D_e = (D^2_{e,m} - D^2_{e,*})^{1/2} \quad \text{with} \quad D_{e,m} = 2(A_e/\pi)^{1/2},$$

where A_e represents the area inside the isophote which contains half flux of the considered region. We have computed the FWHM for many stars with fluxes ranging from 5 to 1000 (arbitrary units). They are closely similar, with a mean value of 3″.1 and a rms dispersion of 0″.2. This value was adopted for $D^2_{e,*}$. Half of the 306 detected H II regions have no measurable diameter. This is due to the rather coarse value for our stellar point spread function and the relatively small intrinsic diameters of the regions.

2.3. *The catalogue (Table 2)*

Positions are given in the sky plane. The coordinate X is positive towards the west direction and the coordinate Y positive towards the north direction.

Column 1: reference number N of the H II region
Column 2 and 3: coordinates X and Y in arcsec with the origin of Table 1
Column 4: total flux in arbitrary units $F = \int E(\mathrm{H}\alpha)\, dA$
Column 5: total surface A measured in (arcsec)^2
Column 6: equivalent diameter D_e in arcsec when measurable
Column 7: localisation in defined structures (L)

NO: north principal arm, SO: south principal arm
N1: north secondary arm, S1: south secondary arm
N2, S2: ramification of the northern (respectively southern) arm,
A: circular ring at the edge of the central disk, B: bar.

2.4. H II *regions properties*

2.4.1. Localization

As can be seen from Figs. 2 and 3, the brightest regions are found either in the bar or in the two principal arms (NO and SO), which thus appear as the main response to the bar perturbation. Other secondary structures are however clearly shown, and are also clearly related to the bar (Fig. 4).

As logarithmic spirals are generally a good representation for the spiral arms, we use a $\log(\varrho, \theta)$ representation of the galaxy plane. This transforms spirals in lines whose slope is the spiral pitch angle. As the arms are accurately symmetric with respect to the bar center, we choose it as the origin of the coordinates for that plane mapping. As shown in Fig. 5, this gives 3 different sets of parallel lines. They correspond respectively to the principal arms NO and SO (pitch angle $15° \pm 3°$), the secondary arms N1 and S1 located inside them (pitch angle $9° \pm 3°$), and to the ramifications N2 and S2 of the main arms (pitch angle $22° \pm 5°$).

It is interesting to notice that the brightest regions are located near bifurcation points, namely at the beginnings of the NO and SO arms and of the N2 and S2 ramifications. Most of the other regions fill a one arcmin radius thickness ring located in the galactic plane at a 1′.8 radius. It is tempting to associate this structure with trapped gas at the outer Lindblad resonance (Combes & Gerin 1985). As we will see in Sect. 3.3, this seems to be the case.

As we see, the spiral structure of NGC 7741 is considerably more complex and more evolved than the basic two-armed grand design generally postulated for barred galaxies.

2.4.2. Fluxes and luminosities

The total flux of the southern and northern arms are equivalent to better than 10% but their distribution is quite dissimilar, as NO is brighter than SO, but N2 is fainter than S2. The global luminosity function of the H II regions is, as usual, quite well represented by a power law, whose coefficient is here $\alpha = 1.7 \pm 0.2$ (Fig. 6). This compares well with similar determinations which range from 1.1 (NGC 2997) to 2.5 (NGC 628). The precision for NGC 7741 is unfortunately quite poor, as faint H II regions numbers are grossly underestimated and many giant regions certainly suffer from superimposition effects.

From a spectroscopic study of the bright H II regions of the bar (number: 151, 152, 153, 154, 156), we have estimated the logarithmic extinction $c(\mathrm{H}\beta)$, assuming an intrinsic $\mathrm{H}\alpha/\mathrm{H}\beta$ ratio of 2.86. This gives the absolute Hα fluxes of the stellar continuum and equivalent width of the Hβ and Hα lines for that regions (Table 3). We have also used it to calibrate the Hα fluxes given in Table 2, Column 4. One unit per (arcsec)^2 in the table corresponds to a flux of $7.7 \pm 1.1\ 10^{-15}$ erg cm^{-2} s^{-1}. With this value we obtain a total Hα flux of $1.05\ 10^{-13}$ erg cm^{-2} s^{-1} for the two regions number 152 and 154. The same flux has been found by Keel (1983) in a 8″.1 central aperture which integrates these two regions.

The total Hα surface emission of the galaxy represents 170 arbitrary units per (arcsec)^2, or a luminosity for $1.7(\pm 0.2) \cdot 10^{40}$ erg s^{-1}. This corresponds to only 1% of the total blue light, which is quite normal for even highly H II region-rich galaxies.

3. Kinematics of the ionized hydrogen

Since a few years, detailed velocity fields of barred galaxies have been obtained with the TAURUS scanning Fabry-Pérot interferometer, e.g. NGC 1365 (Teuben et al. 1986), NGC 1433 (Buta 1986), NGC 6300 (Buta 1987) and NGC 4027 (Pence et al. 1987). A similar instrument, called CIGALE (Boulesteix et al. 1983) has been developed and used by an Observatoire de Marseille team on various galaxies and galactic nebulae. In particular NGC 7741 has been fully scanned in Hα and the results are presented here.

3.1. *Observations and reductions*

The observations were made during a run at the 2.6 m telescope at Burakan Observatory (USSR). With an aperture ratio of f:1.9, the pixel scale on the photon counting camera as 2″.1 × 2″.1. The

1991A&A...241..375D

Table 2. Catalogue of H II regions

N	X	Y	F	A	D_e	L
1	-93.	-51.	10	38	2.5	A
2	-81.	-77.	9	48	*	A
3	-73.	-75.	4	12	*	A
4	-67.	-72.	3	12	*	A
5	-55.	-76.	20	89	4.	S0
6	-44.	-74.	19	57	2.5	S0
7	-56.	-51.	133	56	4.	S2
8	-51.	-49.	21	23	*	S2
9	-64.	-55.	20	68	4.	S2
10	-44.	-52.	88	74	4.	S2
11	-42.	-58.	55	67	4.	S2
12	-40.	-49.	9	8	*	S2
13	-42.	-55.	7	28	*	S2
14	-47.	-61.	22	34	2.5	S2
15	-53.	-67.	18	50	2.5	S2
16	-48.	-58.	7	14	*	S2
17	-48.	-54.	16	26	*	S2
18	-49.	-24.	23	3	*	S2
19	-54.	-32.	34	52	2.5	S2
20	-55.	-37.	4	8	*	S2
21	-45.	-34.	52	68	4.	S2
22	-45.	-27.	15	28	*	S2
23	-49.	-29.	13	22	*	S2
24	-49.	-34.	95	21	*	S2
25	-39.	-34.	11	22	*	S2
26	-39.	-43.	10	21	*	S2
27	-33.	-39.	112	89	2.5	S2
28	-29.	-34.	27	34	2.5	S2
29	-29.	-27.	21	54	4.	S1
30	-25.	-24.	13	22	*	S1
31	-44.	-44.	11	35	*	S2
32	-50.	-39.	5	23	*	S2
33	-61.	-43.	7	30	*	S2
34	-59.	-35.	7	33	2.5	S2
35	-35.	-73.	8	34	*	S0
36	-28.	-78.	14	61	2.5	S0
37	-24.	-66.	16	50	2.5	S0
38	-28.	-64.	4	18	*	S0
39	-21.	-62.	10	40	2.5	S0
40	-20.	-55.	51	59	2.5	S0
41	-26.	-50.	8	27	*	S0
42	-31.	-55.	8	25	*	S0
43	-16.	-68.	6	33	*	S0
44	-18.	-84.	7	35	2.5	S0
45	-24.	-44.	8	24	*	S2
46	-18.	-42.	5	14	*	S2
47	-18.	-38.	3	11	*	
48	-21.	-32.	15	58	2.5	S1
49	-15.	-100.	11	49	*	A
50	-4.	-97.	36	154	6.	A
51	7.	-82.	10	42	*	A
52	4.	-78.	3	20	*	A

Table 2 (continued)

N	X	Y	F	A	D_e	L
53	-9.	-57.	64	58	*	S0
54	-6.	-56.	36	56	2.5	S0
55	-3.	-51.	15	26	*	S0
56	-14.	-62.	4	19	*	S0
57	2.	-46.	43	81	4.	S0
58	2.	-49.	5	16	*	S0
59	11.	-42.	8	19	*	S0
60	7.	-38.	13	41	2.5	S0
61	2.	-39.	6	22	*	S0
62	18.	-46.	39	74	4.	S0
63	12.	-56.	17	74	2.5	S0
64	20.	-45.	12	38	2.5	S0
65	29.	-49.	8	19	*	S0
66	22.	-54.	8	33	*	S0
67	21.	-54.	8	33	2.5	S0
68	26.	-47.	5	11	*	S0
69	20.	-75.	7	25	*	A
70	19.	-80.	4	14	*	A
71	21.	-79.	3	11	*	A
72	30.	-84.	23	63	4.	A
73	29.	-86.	5	21	*	A
74	39.	-76.	7	29	*	A
75	36.	-70.	6	26	*	A
76	37.	-71.	4	11	*	A
77	39.	-69.	2	8	*	A
78	57.	-88.	16	63	4.	A
79	58.	-51.	22	42	*	A
80	54.	-57.	11	42	*	A
81	65.	-53.	9	37	*	A
82	58.	-47.	5	24	*	A
83	38.	-62.	4	21	*	A
84	-5.	-102.	6	27	*	A
85	3.	-61.	4	23	*	S0
86	24.	-60.	6	35	*	S0
87	47.	-53.	46	56	2.5	A
88	43.	-53.	37	63	2.5	A
89	46.	-56.	6	22	*	A
90	44.	-60.	4	21	*	A
91	80.	-50.	4	24	*	A
92	84.	-46.	7	31	*	A
93	37.	-56.	2	15	*	A
94	43.	-39.	9	25	*	A
95	54.	-31.	7	31	*	A
96	46.	-37.	57	88	5.	A
97	46.	-44.	11	37	*	A
98	52.	-39.	7	30	*	A
99	58.	-39.	6	33	*	A
100	67.	-42.	81	108	4.	A
101	73.	-29.	6	20	*	A
102	67.	-28.	51	115	5.	A
103	75.	-24.	62	26	*	A
104	55.	-25.	4	23	*	A

Table 2 (continued)

N	X	Y	F	A	D_e	L
105	38.	-30.	5	25	*	
106	9.	-32.	25	55	2.5	S0
107	13.	-25.	36	40	*	S0
108	14.	-21.	25	36	*	S0
109	25.	-31.	18	61	4.	S0
110	15.	-31.	11	37	2.5	S0
111	20.	-26.	45	64	2.5	S0
112	22.	-23.	22	62	4.	S0
113	3.	-23.	8	42	*	S1
114	-11.	-30.	5	28	*	S1
115	-9.	-31.	7	38	*	S1
116	-4.	-38.	10	44	2.5	
117	-4.	-43.	4	21	*	S0
118	39.	-18.	12	65	2.5	S0
119	46.	-19.	21	64	2.5	
120	21.	-12.	119	58	*	S0
121	25.	-13.	38	28	*	S0
122	16.	-16.	22	67	4.	S0
123	26.	-7.	19	28	2.5	S0
124	38.	-5.	15	28	*	S0
125	57.	2.	16	76	4.	
126	70.	-7.	5	26	*	A
127	47.	-4.	4	19	*	
128	44.	-10.	16	50	2.5	
129	53.	11.	14	52	2.5	
130	45.	10.	64	67	2.5	
131	70.	16.	15	75	4.	N2
132	65.	20.	13	64	4.	N2
133	52.	17.	6	32	*	
134	44.	16.	8	23	*	
135	44.	1.	8	37	2.5	
136	25.	-1.	7	52	4.	S0
137	30.	2.	38	28	2.5	S0
138	24.	7.	124	78	4.	S0
139	26.	5.	109	59	4.	S0
140	34.	4.	83	84	5.	S0
141	29.	12.	32	61	4.	S0
142	21.	20.	13	20	*	N1
143	18.	17.	23	34	2.5	N1
144	18.	3.	49	46	4.	B
145	24.	-1.	31	37	2.5	B
146	8.	12.	23	46	2.5	
147	10.	6.	14	23	*	B
148	1.	14.	63	93	5.	
149	-40.	-11.	12	23	*	N0
150	16.	-9.	12	23	*	S1
151	10.	0.	189	45	2.5	B
152	2.	0.	373	50	2.5	B
153	5.	0.	285	47	2.5	B
154	-3.	0.	341	56	2.5	B
155	-1.	-5.	124	44	2.5	B
156	-7.	0.	159	50	4.	B

Table 2 (continued)

N	X	Y	F	A	D_e	L
157	-14.	-10.	55	60	4.	B
158	-13.	6.	26	39	2.5	B
159	-11.	11.	5	14	*	
160	-10.	17.	6	21	*	
161	-10.	-2.	111	72	5.	B
162	-16.	18.	10	36	*	N1
163	-20.	9.	26	52	2.5	N1
164	-23.	-3.	140	93	5.	B
165	-26.	-9.	248	123	4.	B
166	-32.	-10.	57	59	4.	B
167	-34.	-20.	20	71	4.	S1
168	-41.	-16.	23	52	2.5	S1
169	-44.	-12.	8	20	*	S1
170	-50.	-6.	40	59	2.5	S2
171	-59.	-15.	16	49	2.5	S2
172	-67.	-25.	14	77	4.	S2
173	-76.	-17.	4	21	*	A
174	-59.	-9.	58	69	2.5	S2
175	-57.	-1.	52	50	2.5	S2
176	-62.	3.	29	45	*	S2
177	-56.	-1.	44	65	4.	S2
178	-57.	12.	8	37	2.5	
179	-34.	15.	200	70	2.5	N0
180	-35.	7.	961	181	2.5	N0
181	-43.	6.	19	62	2.5	N0
182	-40.	-4.	165	143	5.	N0
183	-32.	-4.	48	92	5.	B
184	-15.	-20.	5	23	*	
185	-70.	2.	6	41	*	A
186	-77.	0.	6	27	*	A
187	-83.	4.	6	35	*	A
188	-87.	9.	4	22	*	A
189	-92.	9.	4	19	*	A
190	-33.	8.	84	36	*	N0
191	77.	19.	8	44	*	A
192	84.	16.	5	28	*	A
193	85.	-4	5	24	*	A
194	87.	-1.	5	28	*	A
195	92.	-1.	4	20	*	A
196	89.	-11.	7	35	*	A
197	104.	-2.	8	35	2.5	A
198	-32.	-94.	9	45	2.5	A
199	-6.	-20.	8	34	2.5	
200	57.	18.	10	40	2.5	N2
201	56.	31.	8	42	*	N2
202	72.	35.	9	48	2.5	A
203	84.	38.	9	50	2.5	A
204	101.	37.	12	56	2.5	A
205	79.	44.	24	40	*	A
206	75.	43.	16	35	*	A
207	67.	45.	13	52	2.5	A
208	72.	49.	42	73	4.	A

Table 2 (continued)

N	X	Y	F	A	D_e	L
209	78.	55.	7	39	*	A
210	84.	54.	7	36	2.5	A
211	90.	62.	4	23	*	A
212	97.	64.	6	30	*	A
213	48.	56.	32	73	2.5	N2
214	45.	46.	32	68	4.	N2
215	51.	37.	18	73	4.	N2
216	56.	40.	22	95	4.	N2
217	52.	47.	12	30	*	N2
218	60.	50.	4	22	*	A
219	38.	28.	9	43	2.5	
220	29.	26.	24	78	2.5	
221	34.	45.	18	80	4.	N2
222	26.	44.	11	51	2.5	N2
223	23.	50.	43	76	2.5	N2
224	18.	56.	48	85	2.5	N2
225	29.	60.	14	43	*	N2
226	31.	66.	14	37	*	N2
227	22.	67.	9	37	*	N2
228	14.	28.	8	43	*	N1
229	-3.	25.	8	35	*	N1
230	2.	32.	7	33	*	N1
231	-4.	34.	9	41	2.5	N1
232	0.	42.	13	65	2.5	
233	9.	46.	7	44	*	N2
234	-6.	54.	62	114	2.5	N0
235	6.	63.	16	59	4.	N0
236	7.	69.	18	33	2.5	N0
237	13.	78.	44	58	4.	N0
238	16.	82.	8	22	*	N0
239	24.	83.	22	27	*	N0
240	28.	86.	43	45	4.	N0
241	26.	68.	7	33	*	N2
242	39.	95.	35	28	2.5	N0
243	25.	95.	58	58	4.	N0
244	2.	79.	10	45	2.5	N0
245	-7.	68.	11	45	2.5	N0
246	-6.	76.	9	55	2.5	N0
247	-10.	37.	13	47	2.5	
248	-13.	51.	11	39	2.5	N0
249	-11.	25.	6	26	*	N1
250	-18.	24.	7	26	*	N1
251	-34.	21.	50	39	2.5	N0
252	-40.	24.	32	43	*	N0
253	-36.	30.	86	75	4.	N0
254	-29.	28.	33	52	4.	N0
255	-28.	34.	48	56	2.5	N0
256	-36.	38.	27	50	2.5	N0
257	-42.	33.	16	32	2.5	N0

Table 2 (continued)

N	X	Y	F	A	D_e	L
258	-24.	41.	30	97	4.	N0
259	-34.	42.	18	86	4.	N0
260	-26.	62.	24	38	6.5	A
261	-23.	85.	9	55	2.5	A
262	-22.	92.	22	113	5.	A
263	3.	96.	24	114	5.	A
264	14.	58.	8	38	*	N2
265	-41.	54.	9	46	2.5	A
266	-46.	48.	10	45	2.5	A
267	-55.	42.	15	53	4.	A
268	-54.	65.	12	52	2.5	A
269	-61.	61.	13	64	4.	A
270	-65.	58.	11	57	2.5	A
271	-66.	34.	7	53	*	A
272	13.	76.	7	18	*	N0
273	-59.	-6.	10	22	*	S2
274	-37.	17.	15	40	*	N0
275	-35.	24.	12	11	*	N0
276	-45.	-90.	4	25	*	A
277	-53.	-93.	5	34	*	A
278	-74.	71.	12	68	4.	A
279	-4.	57.	18	28	*	N0
280	44.	44.	8	19	*	N2
281	-94.	99.	10	47	2.5	
282	-58.	30.	6	30	*	A
283	-44.	21.	5	30	*	N0
284	-50.	22.	4	22	*	
285	-54.	20.	3	18	*	
286	-53.	25.	4	30	*	
287	4.	119.	18	96	5.	A
288	15.	134.	7	37	*	A
289	10.	135.	6	33	*	A
290	-6.	133.	27	138	5.	A
291	-20.	134.	14	69	4.	
292	32.	41.	4	20	*	N2
293	5.	67.	14	42	4.	N0
294	-59.	125.	11	59	4.	
295	18.	57.	30	33	*	N2
296	-79.	57.	7	37	*	A
297	-81.	70.	6	36	*	A
298	-54.	102.	8	36	2.5	A
299	-55.	99.	5	24	*	A
300	-52.	49.	4	27	*	A
301	-66.	-22.	6	30	*	S2
302	-27.	8.	3	11	*	N1
303	46.	33.	13	45	2.5	N2
304	34.	29.	5	23	*	
305	28.	17.	6	30	*	N1
306	7.	80.	9	22	*	N0

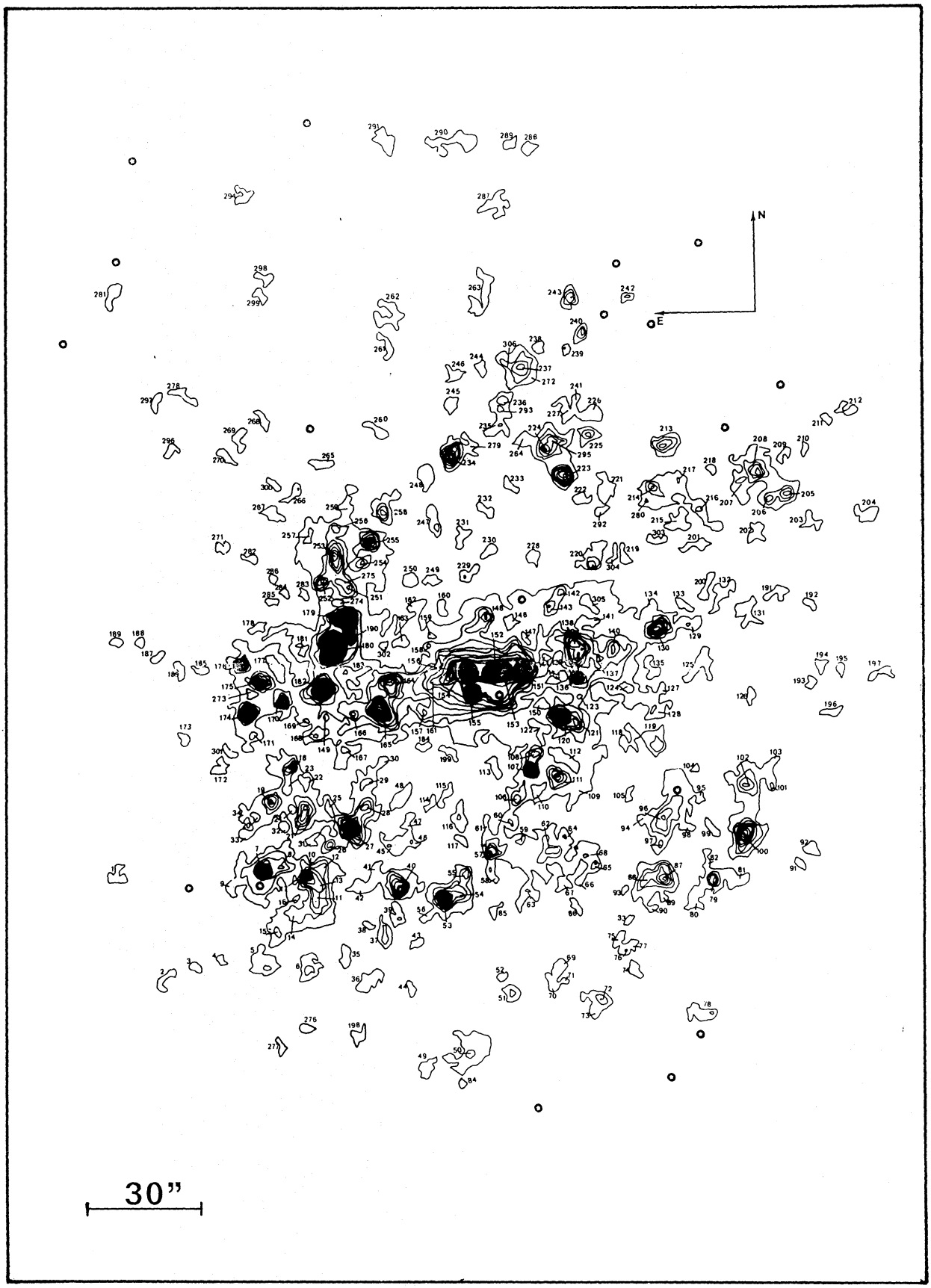

Fig. 2. Identification of the 306 measured H II regions. The isophotes are equally spaced in intensity. Bright stars are indicated as circles

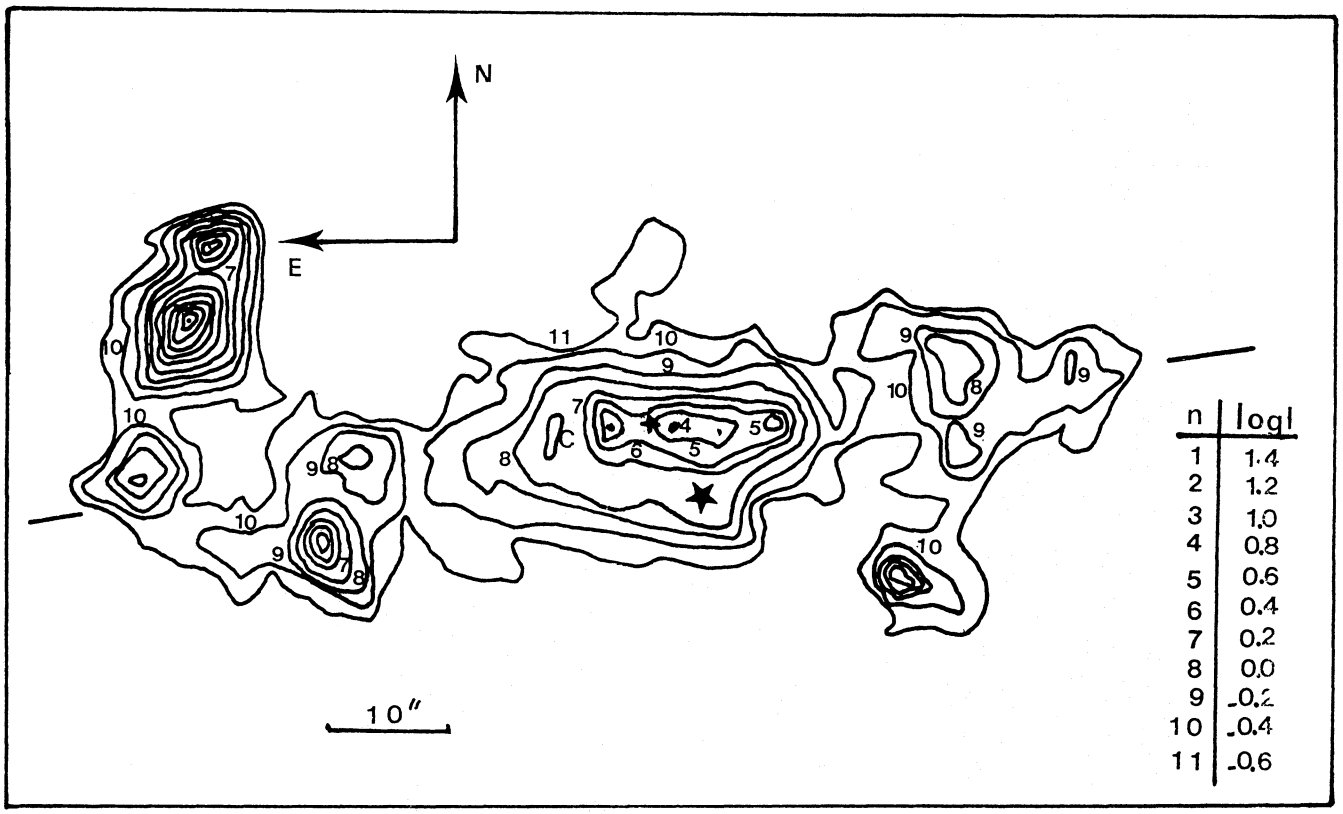

Fig. 3. Hα isophotes of the bar of NGC 7741, "C" is the center of the bar [offset by 7″ from the origin of the coordinates (+)] and the center of the outer B luminosity isophotes

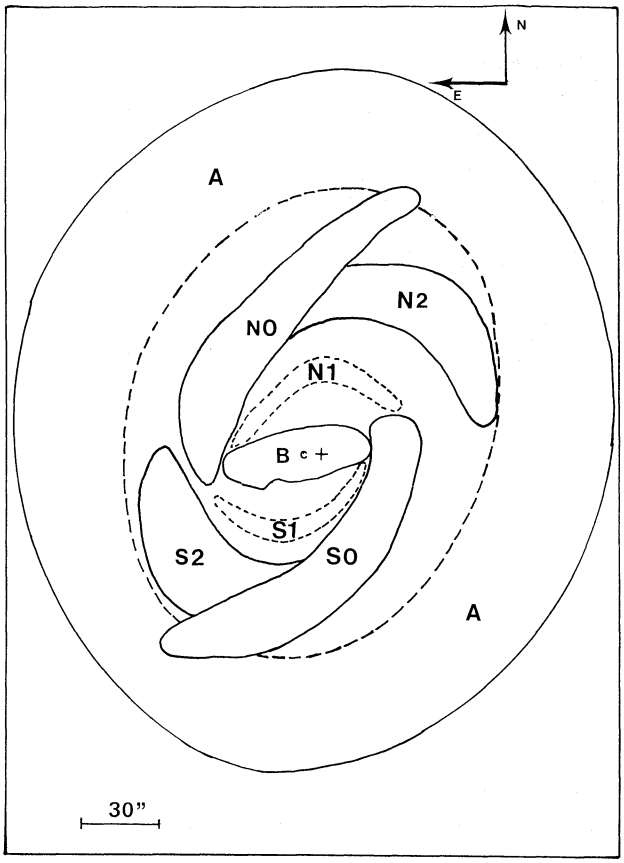

Table 3. Photometric data of the central H II regions of the bar

Region number	X (″)	$W(H\beta)$ (Å)	$W(H\alpha)$ (Å)	$C(H\beta)$	$I(H\beta)$ (10^{-14} erg cm^{-2} s^{-1})	$I(H\alpha)$ (10^{-14} erg cm^{-2} s^{-1})
151	+10	11	52	0.00	1.2	3.2
152	+ 2.5	7	66	0.67	1.1	5.8
153	+ 5.0	9	63	0.27	1.2	4.7
154	− 3.5	6	68	0.92	0.9	4.7
156	− 7.0	8	48	0.06	1.0	2.5

interferometer's order was 796 at Hα, providing a free spectral range of 376 km s^{-1}. It was covered in 21 steps, and gives an instrumental resolution of 25 km s^{-1}. The guiding system performance was quite poor and led to severely trailed images during the scanning (see Marcelin et al. 1986 for details). This was however successfully software-corrected by E. Le Coarer for both spatial and spectral trailing effects.

Then the general software package developed by J. Boulesteix produced a data cube with 2 spatial coordinates and one for velocity (or wavelength). From it, iso-radial velocity, and Hα and stellar continuum images have been extracted. The reductions have been conducted as described by Laval et al. (1987) in partic-

Fig. 4. Schematic map of the main and seondary structures of NGC 7741 detected with the Hα exposure (bar, arms, outer ring)

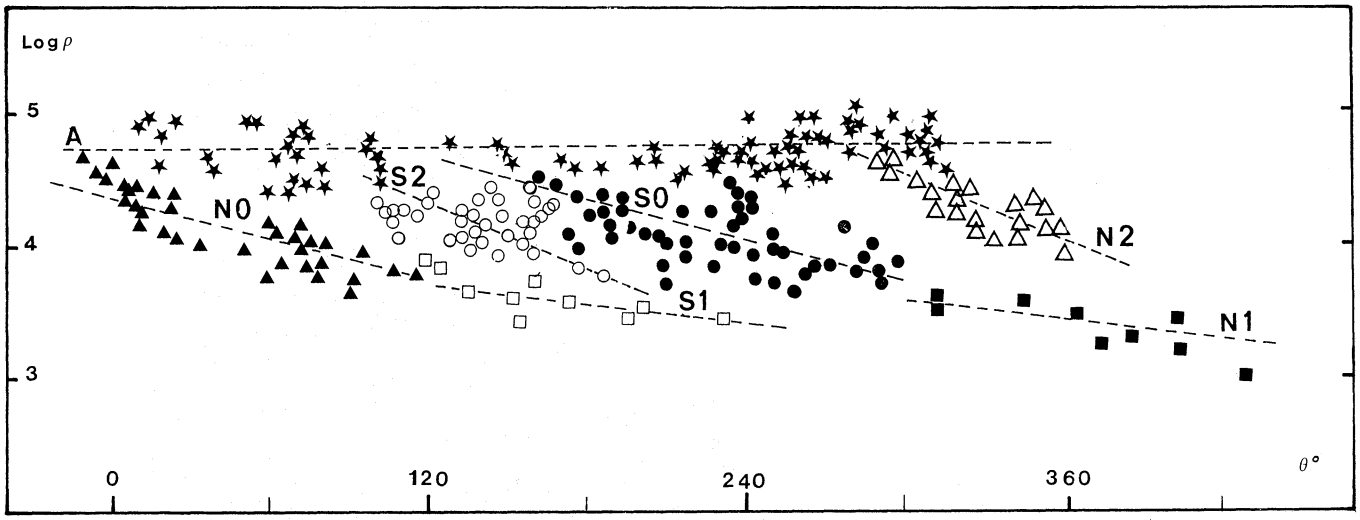

Fig. 5. Logarithmic representation of the spiral structures from positions of the H II regions

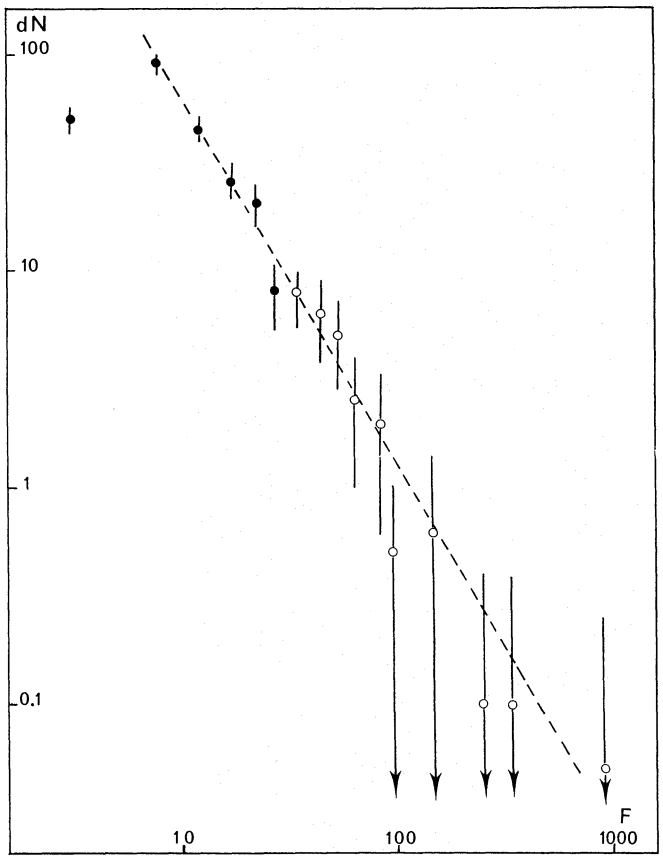

Fig. 6. Luminosity function from the 306 H II regions identified. Each point is the mean number of regions per five arbitrary units of flux (F). When the statistics are insufficient, the number is calculated from a larger interval (and represented by an empty circle)

ular for night sky emission lines subtraction. As the OH line at 652.72 nm is exactly in coincidence with the radial velocities of the most distant southern H II regions, no measurement of these regions have been attempted.

3.2. *Radial velocity field*

A two-dimension map of 2500 radial velocities superposed on Hα distribution is given in Fig. 7a. With the representation adopted, each symbol corresponds to a 15 km s^{-1} step from 640 km s^{-1} to 850 km s^{-1}. The radial velocity of the center of the galaxy is here 752 km s^{-1} (very close to the value of 755 km s^{-1} found previously by DM).

Much more clearly than in DM, a large S-shaped distortion of the isoradial velocity curves is seen along the bar (Fig. 7b). A 68 km s^{-1} kpc^{-1} gradient is measured across the bar near the center. A pseudo-ring at +60 km s^{-1} surrounds the empty zone of ionized hydrogen located at the north of the bar while an equivalent southern zone may exist at −75 km s^{-1}.

3.3. *Axisymmetric model*

The rotation curve $\Theta(\varrho)$ up to $\varrho = 2'$ in the northern side and up to $\varrho = 1'.2$ in the southern side has been first computed from the radial velocity of all points (375) found at less of ± 15° from the major axis (Fig. 8). It has then been interactively corrected in the gas flow model described below to get the best possible fit of the radial velocities very close to the major axis. It turns to be well represented by a Kuz'min-Toomre disk for which:

$$\Theta^2(\varrho) = \frac{A^2 \varrho^2}{(a^2 + \varrho^2)^{3/2}}$$

with $A = 220$ km s^{-1} arcmin^{-1} and $a = 1'.1$. An important parameter for deriving a dynamical model is the value of the pattern speed and consequently the type of resonance associated with the end of the bar. This is usually discussed with the help of the familiar resonance curves $\Omega + \kappa/m$.

Unfortunately, because of the small extent of the ionized gas, we have no knowledge of the rotation curve beyond a 2'.0 radius. However, Shostak (1975) has measured the integrated H I 21 cm

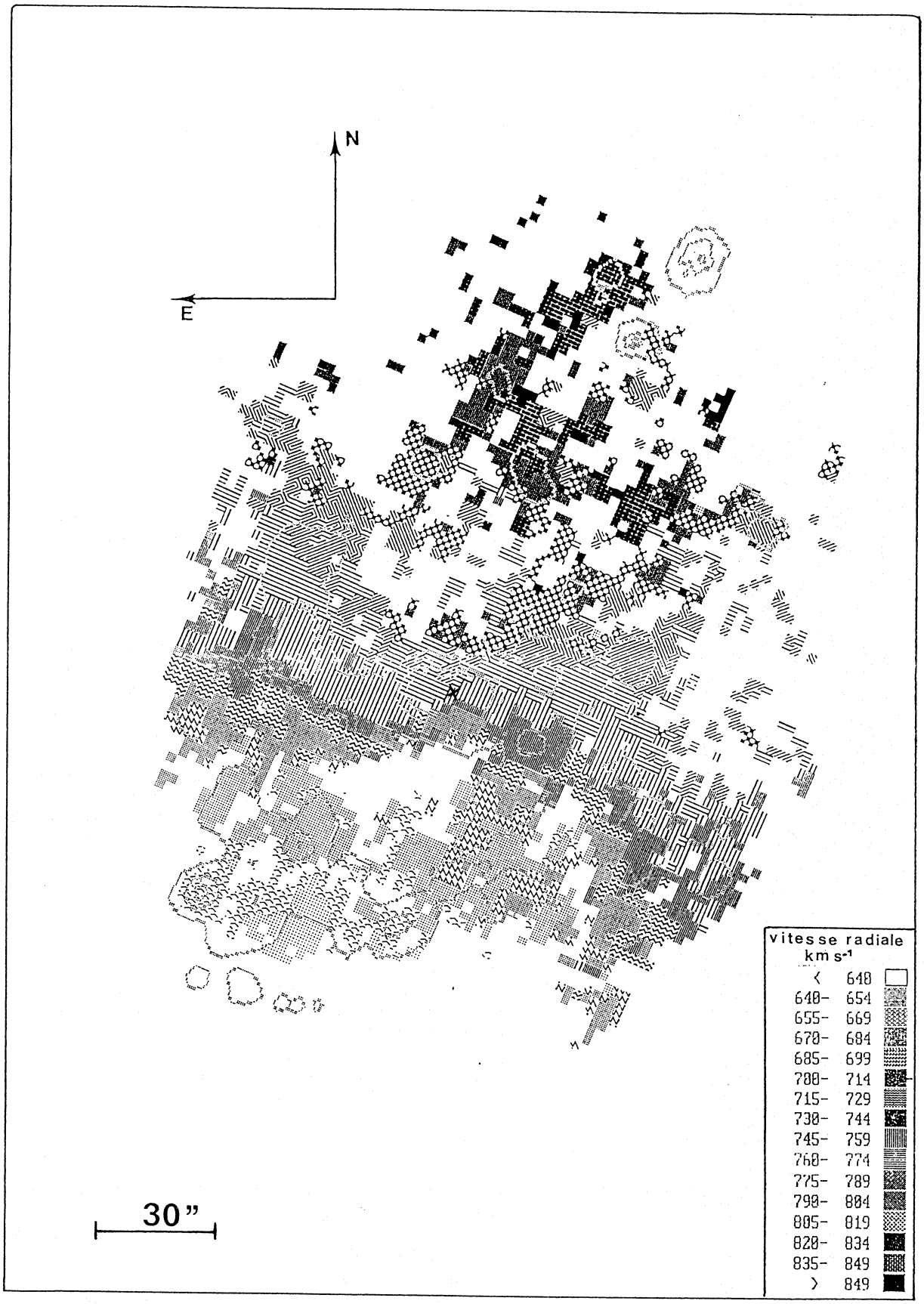

Fig. 7a. Coded isoradial velocity map in the plane of the sky where the 2500 pixels measured are visible. Intervals are of 15 km s^{-1}. The origin of the coordinates is indicated by a cross

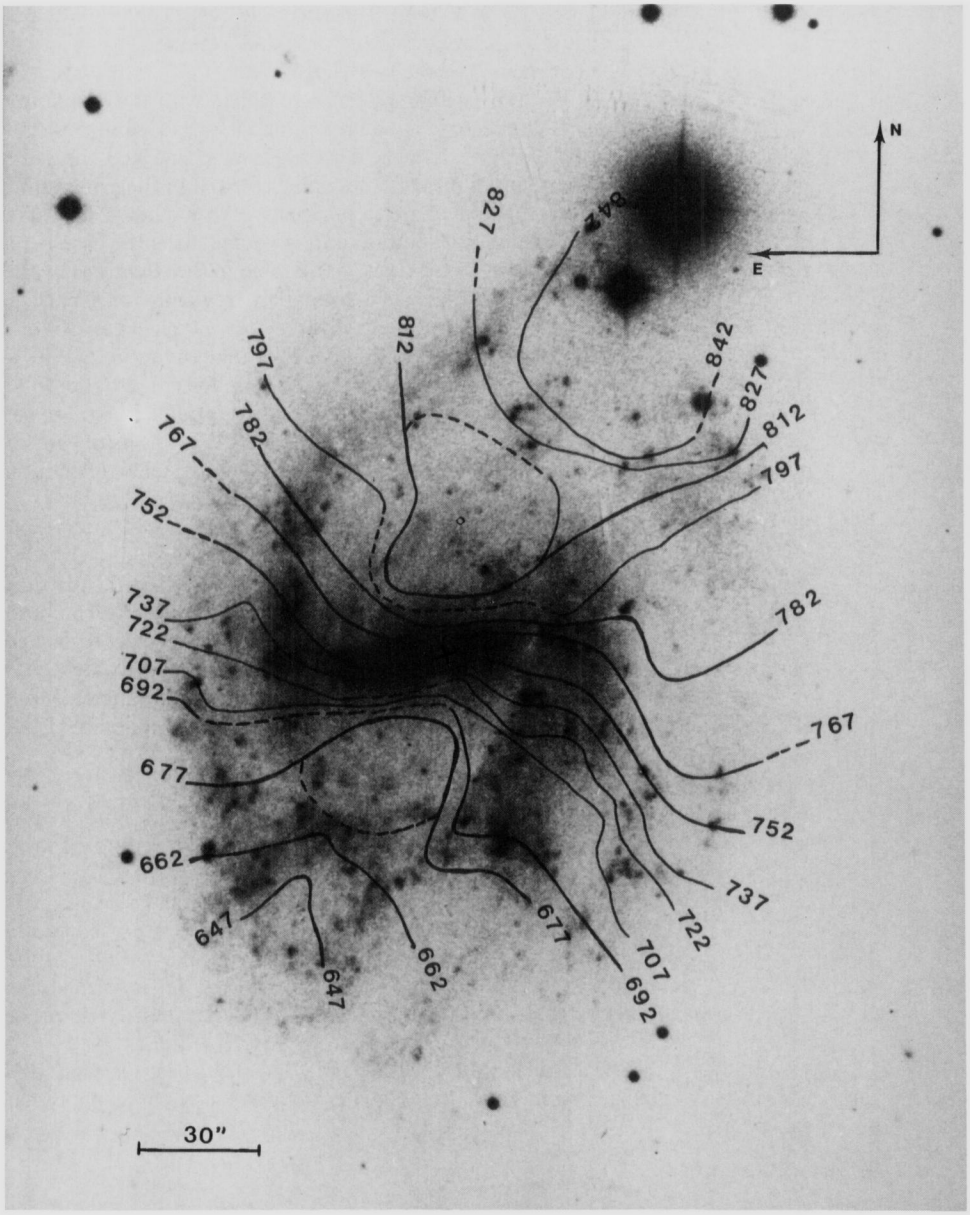

Fig. 7b. Isoradial velocity curves superimposed on a photograph of NGC 7741 published in the Atlas of Galaxies edited by NASA (1988)

profile of NGC 7741 with the 300 feet NRAO radiotelescope. He found the double-peaked curve characteristic of galaxies with flat rotation curves. The distance between the two peaks is $\Delta V = 153$ km s^{-1}, which translated to a maximum rotation velocity gives: $\Theta_M = 153/2 \sin i = 108$ km s^{-1}. Bottinelli et al. (1983) have also derived the maximum rotation velocity from a statistically valid technique and using Nançay data. They found $\Theta_M = 115$ km s^{-1}.

Our analytical expression gives $\Theta_M = 130$ km s^{-1} at 1'.5 radius (in good agreement with the northern side of the rotational curve). We have thus computed $\Omega + \kappa/m$ curves with m_∞, $m = 2$ and $m = -4$ from the analytical expression up to $\varrho = 1'.5$ and a flat extrapolation beyond. They are given in Fig. 9. It is rather tempting to put the end of the bar at the $m = -4$ ultra-harmonic resonance (UHR). This gives corotation at 1'.65, very close to the end of the strong spiral structure, and the outer Lindblad resonance at 2'.35, in good agreement with the extension of the strong H II regions.

While corotation at the end of the bar is generally preferred on a theoretical basis (see e.g. Athanassoula et al. 1982; Contopoulos 1988), UHR still seems a valid option. However, as pointed to us by the referee, it is very difficult from hydrodynamical models to get a robust spiral structure inside corotation in the presence of a strong bar. This strongly push to put the end of the bar at corotation. The end of the spiral structure is then at the $m = 2$ Lindblad resonance. Isolated patches of H II regions do occur outside, but mainly on the northern side, and could be accounted for as a one-arm component (or even as being no part of any global structure).

3.4. Dynamical model

We have used the linearized Euler equations, in the absence of shocks, given by Athanassoula (1978), which give the rotation velocity and expansion velocity components of order m(even), $U_{\theta,m}(\varrho)$ and $U_{r,m}(\varrho)$. The axisymmetric functions $\Theta(\varrho)$ and $\kappa(\varrho)$

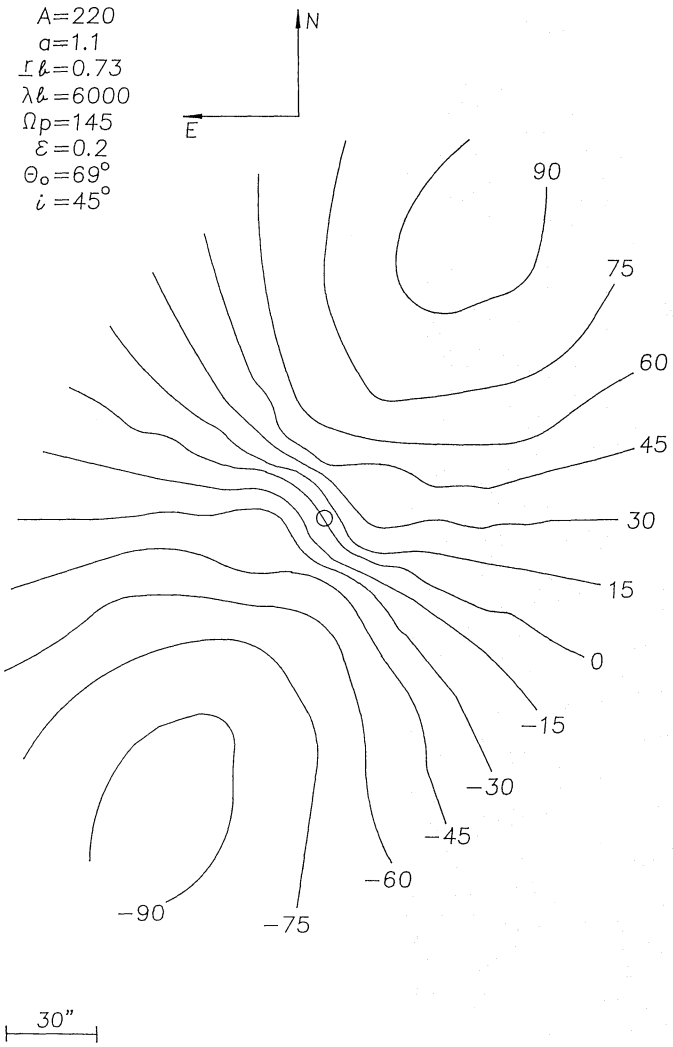

Fig. 7c. Best fit isovelocities given by the dynamical model. Scales and orientations are the same in the three Figs. 7a, 7b and 7c

computed in 3.3. were used. The offsetting of the center of the bar with regard to the center of the disk was neglected.

The parameters in the model are:

– The pattern angular velocity Ω_p which, with the corotation at the end of the bar, is equal to 145 km s^{-1} (arcmin)$^{-1}$. It is significantly higher than the DM value who adopted the same hypotheses. This translates to a value of ~ 80 in the same units. This kind of change can easily happen with new data having a much better spatial resolution and coverage, as is the case here.

– The viscosity of the flow, represented in the equations by the imaginary component $i\varepsilon$ of the angular frequency of a particle passing through the bar. We have taken for ε a typical value of 0.2.

– The (even) Fourier components of the gravitational potential of the bar, which can be computed from the true axial ratio of the bar, equal to 0.23, and its density law. It is quite difficult to get the real mass density law of the bar of NGC 7741 as its old stellar component is heavily contaminated by strong stellar formation down to the very center, probably associated to gas spiraling in the absence of an ILR. As in DM, we have chosen a constant (spatial) density bar for this underlying component.

The computed velocity field was then projected on the plane of the sky, using the known geometrical parameters (inclination $i = 45°$, angle of the major axis of the bar with respect to line of nodes $\theta_0 = 69°$). A best fit with the observed velocity field was then searched, using the mass of the bar as a free parameter. More specifically, we used the normalizing coefficient λ_b, defined by:

$$\lambda_b = 0.0172 f_b I_b q_{ab} r_b \text{ km}^2 \text{ s}^{-1},$$

where f_b is the blue M/L ratio of the bar, I_b its blue central luminosity ($= 20.42$ mag (arcsec)$^{-2}$), q_{ab} its apparent axial ratio ($= 0.30$), and r_b its radius ($= 0'.73$).

The best fit is found for $\lambda_b = 6000$ (± 1000 at 1σ) km s^{-2}. It is shown in Fig. 7c. While some details of the observed radial velocity field – such as the asymmetry between the two sides of the major axis cannot obviously be reproduced – the major features and especially the characteristic kink in the isovelocity curves in the region of the bar are present.

The use of a smaller viscosity coefficient has been checked: this changes mainly the intermediate radial velocity curves (between

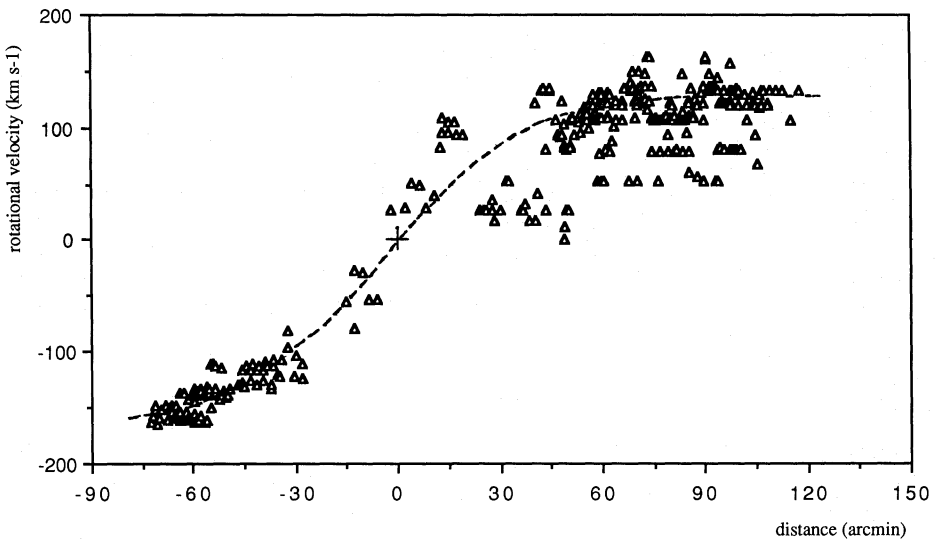

Fig. 8. Rotation curve of NGC 7741. The rotational velocities are computed from the radial velocity of all points found at less of $\pm 15°$ from the major axis. Points of the upper quadrant come from the northern side of the galaxy

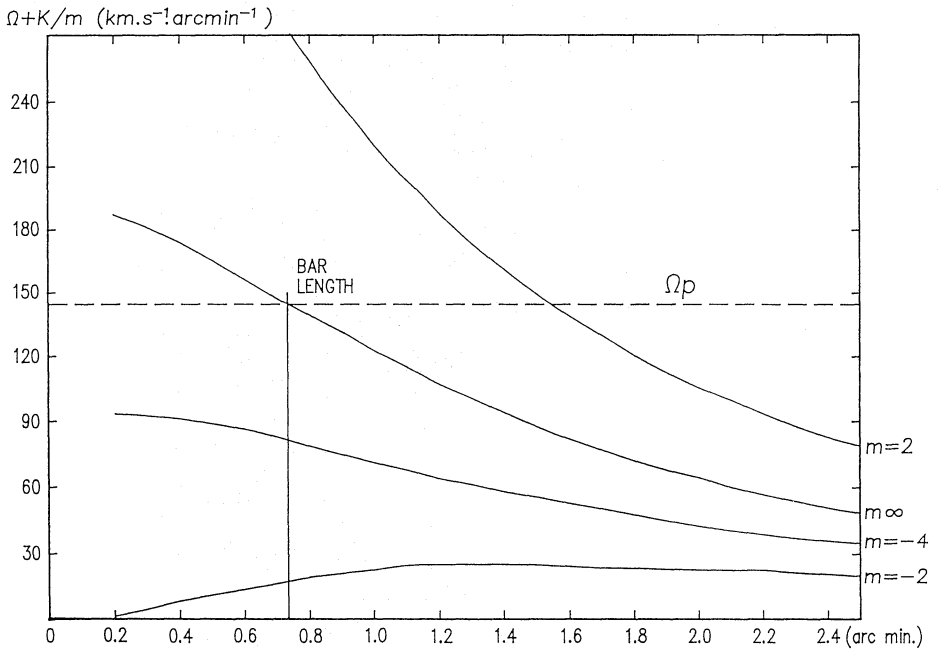

Fig. 9. Resonance curves $\Omega + \kappa/m$ with $m = 2, \infty, -4, -3$, and -2. The bar length is indicated by a solid line and the proposed pattern angular velocity Ω_p by a dashed line

± 70 and ± 50 km s^{-1}) which then are shifted too much near the center of the galaxy.

The total mass of the (homogeneous) bar is:

$$M_b = \frac{2\pi}{3} f_b I_b q_{ab} r_b^2$$

or,

$$M_b = \frac{2\pi}{3} \frac{1}{0.0172} \lambda_b r_b .$$

With a distance modulus of 30.11 (Bottinelli et al. 1984), $r_b = 2234$ pc. For $\lambda_b = 6000$ (± 1000 at 1σ) km^2 s^{-2}:

$$M_b = 1.64(\pm 0.30)\ 10^9\ M_\odot .$$

This can be compared to the mass of the asymmetric component inside the radius of the bar, which is:

$$M_d = 7.1\ 10^5\ A^2\ \ 1 - \frac{1}{\sqrt{1 + \left(\frac{r_b}{a}\right)^2}}$$

or,

$$M_d = 5.7\ 10^9\ M_\odot .$$

The M_b/M_d ratio is thus around 30%. This value is fully independent of the distance scale assumed. We have assumed a constant spatial density law for the bar. This means that its computed mass ratio is in fact a lower limit.

We also run models with the $m = 4$ ultra-harmonic resonance at the end of the bar. The resulting velocity field is quite similar, but a factor of 2 decrease in the mass of the bar is needed for a good fit.

3.5. *Discussion*

The present modelization of the gas flow was made under the assumptions of a linear perturbation of the total gravitational potential by the bar, and of the absence of shocks.

To check the linear assumption, we compute the relative perturbation of the radial forces due respectively to the bar and to the axisymmetric component. It is maximum along the major axis of the bar and reasonably low (20 to 40%) for $\varrho > 0'.2$.

As there is no dust lanes inside the bar, it is indeed reasonable to assume the absence of large-scale shocks. On the other hand, such shocks probably occur in the main spiral arms. However, our simplified model does not even take into account the spiral arms perturbation. This is probably not too serious as no strong effect associated with these arms is apparent on the velocity field, a result not too surprising for a late-type galaxy with broad spiral arms.

In conclusion, through the use of a much better spatial coverage in radial velocities, the S-distortion due to the bar forcing is fully confirmed. A modelization of the gas flow shows that this can be reproduced with a moderately massive bar, with a mass ratio, relative to its surrounding disk of 30%.

Acknowledgements. The observations during summer 1985, were made possible through the generous offer of telescope time by the Special Astronomical Observatory at the Byurakan Observatory (USSR). They were supported by the Institut National des Sciences de l'Univers (France) and the Academy of Sciences of the Soviet Union. We are indebted to the referee (F. Combes) for very valuable help about the dynamical analysis and to engineer J. A. Fort and technicians. A. Viale and P. Joulié for their assistance.

References

Athanassoula E., 1978, A & A 69, 395
Athanassoula E., Bosma A., Crézé M., Schwarz M., 1982, A & A 107, 101
Bottinelli L., Gouguenheim L., Paturel G., de Vaucouleurs G., 1983, A & A 118, 4
Bottinelli L., Gouguenheim L., Paturel G., de Vaucouleurs G., 1984, A & AS 56, 381

Boulesteix J., Georgelin Y. P., Marcelin M., Monnet G., 1983, SPIE Conf. Inst. Astron. Vol. 445, 37
Buta R., 1986, ApJS 61, 631
Buta R., 1987, ApJS 64, 383
Combes F., Gerin M., 1985, A & A 150, 327
Contopoulos G., A & A 201, 44
Deharveng L., Caplan J., Lequeux J., Azzopardi M., Breysacher J., Tarenghi M., Westerlund B., 1988, A & AS 73, 407
Duval M. F., Monnet G., 1985, A & AS 61, 141
Kalnajs A., 1978, IAU Symp. No. 77, Reidel, Dordrecht, p. 113
Keel W., 1983, ApJS 52, 229
Laval A., Boulesteix J., Georgelin Y. M., Marcelin M., 1987, A & A 175, 199
Marcelin M., Gondoin Ph., 1983, A & AS 51, 353
Marcelin M., Le Coarer E., Boulesteix J., Georgelin Y., Monnet G., 1986, A & A 179, 101
Pence W. D., Taylor K., Freeman K. C., de Vaucouleurs G., Atherton P., 1988, ApJ 326, 564
Petit H., Sivan J. P., Karachentsev I. D., 1988, A & AS 74, 475
Petrou M., Papayannopoulos T., 1986, MNRAS 219, 157
Shostak G. S., 1975, ApJ 198, 527
Teuben P. J., Sanders R. H., Atherton P. D., Van Albada G. D., 1986, MNRAS 221, 1
Tully R. B., 1988, Nearby Galaxies Catalogue, Cambridge University Press, Cambridge